

Deploying Federated Learning in Large-Scale Cellular Networks: Spatial Convergence Analysis

Zhenyi Lin, Xiaoyang Li, Vincent K. N. Lau, Yi Gong, and Kaibin Huang

Abstract

The deployment of federated learning in a wireless network, called *federated edge learning* (FEEL), exploits low-latency access to distributed mobile data to efficiently train an AI model while preserving data privacy. In this work, we study the spatial (i.e., spatially averaged) learning performance of FEEL deployed in a large-scale cellular network with spatially random distributed devices. Both the schemes of digital and analog transmission are considered, providing support of error-free uploading and over-the-air aggregation of local model updates by devices. The derived spatial convergence rate for digital transmission is found to be constrained by a limited number of active devices regardless of device density and converges to the ground-true rate exponentially fast as the number grows. The population of active devices depends on network parameters such as processing gain and signal-to-interference threshold for decoding. On the other hand, the limit does not exist for uncoded analog transmission. In this case, the spatial convergence rate is slowed down due to the direct exposure of signals to the perturbation of inter-cell interference. Nevertheless, the effect diminishes when devices are dense as interference is averaged out by aggressive over-the-air aggregation. In terms of learning latency (in second), analog transmission is preferred to the digital scheme as the former dramatically reduces multi-access latency by enabling simultaneous access.

I. INTRODUCTION

The availability of enormous data at edge devices motivate the deployment of machine-learning algorithms at the network edge to distill the data into *artificial intelligence* (AI). The trained AI models are expected to enable a wide range of next-generation mobile applications such as autonomous driving and augmented reality. Fast growing relevant research has led to the

Z. Lin and K. Huang are affiliated with The University of Hong Kong, Hong Kong. Z. Lin is also with the Dept. of EEE at Southern University of Science and Technology (SUSTech), China. X. Li and Y. Gong are with the same institute. V. K. N. Lau is with the The Hong Kong University of Science and Technology, Hong Kong. Corresponding authors: K. Huang (Email: huangkb@eee.hku.hk), Y. Gong (Email: gongy@sustech.edu.cn)

emergence of a new area called *edge learning* [1], [2]. In this area, federated learning is perhaps the most widely studied framework due to its feature of preserving data privacy by avoiding their uploading. To this end, a model-training task is distributed over devices using the iterative algorithm of *stochastic-gradient descent* (SGD) [3]. A main vein of research on edge learning concerns efficient implementation of federated learning in wireless systems, call *federated edge learning* (FEEL). In this work, we study the performance of FEEL in a large-scale cellular network where inter-cell interference is present. The results help crystalizing the effects of network parameters on the (model) convergence rate.

In the area of FEEL, recent years have seen the development of diversified approaches for overcoming the communication bottleneck, which is caused by the uploading of high-dimensional model updates from multiple devices to a server. One approach is efficient joint management of communication-and-computation resources via designing scheduling and bandwidth allocation to accelerate convergence [4]–[7]. From the theoretic perspective, researchers have attempted to shed light on the fundamental question of how many devices are needed for providing a guarantee on learning performance within a finite time duration [8]. An alternative approach is to realize “over-the-air aggregation” of local model updates so as to support simultaneous access by many devices [9], [10]. The core idea is to adopt analog transmission so as to exploit the waveform-superposition property of a multi-access channel. The versatility and efficiency of over-the-air aggregation has been improved by the development of numerous relevant techniques including digital aggregation [11], gradient compression [10], power control [12], and beamforming [13]. Another approach is source compression. Some existing techniques exploit local-model sparsity [14] or enable efficient model quantization [15].

In view of prior work, most results assume single-cell systems. The topic of deploying FEEL in a large-scale network remains one largely unexplored. In this scenario, learning performance is affected by inter-cell interference as well as network configurations. Recently, some initial work has accounted for such an effect in designing device-scheduling schemes [16]. While the work points to the important direction of FEEL networking, many fundamental questions remain unanswered. In particular, a question of our interest is how the convergence depends on the network parameters (i.e., device density, cell sizes, and coding rates), which parameterize the interference distribution.

A standard approach of characterizing the effect of inter-cell interference on network performance, which is also adopted in this work, is to model the randomly located network nodes

(devices or base stations) as spatial point processes such as a *Poisson point process* (PPP) or its derivatives [17]. Consequently, the interference power can be modelled as a shot-noise process, referring to a sum over a PPP [18]. Then the study of network performance is reduced to the equivalent analysis of the expected performance of a *typical cell*, which results from uniformly sampling all cells, over the distributions of interference, channels, and nodes [17]. Such analysis leverages a rich set of results from the stochastic-geometry theory [19]. The tractability brought by the theory has motivated many researchers to use it as a tool to study the performance of a wide range of wireless networks such as cellular networks (see e.g., [20]), cooperative networks (see e.g., [21]), heterogeneous networks (see e.g., [22], [23]), and most recently unmanned aerial vehicle networks [24]. Most existing work is based on the classic “communication-and-computation separation” approach. To be specific, the considered networks aim at providing generic radio-access services to users or sensors without concerning their applications. The corresponding design objective is to ensure the required quality-of-service, network throughput or coverage [17]. In contrast, the study of a FEEL network, referring to a network supporting the FEEL application, should adopt a learning-related metric for network performance such as the proposed metric of convergence rate in a typical cell, termed *spatial convergence rate*. The corresponding network-performance analysis is differentiated from existing analysis in its interplay of stochastic geometry and learning theories, which is a key feature of current analysis.

In this work, we consider a large-scale network with hexagonal cells and devices distributed following a PPP. FEEL is deployed in a typical cell. For the reason, the corresponding model convergence is termed *spatial convergence*. Uplink transmission by each device is based on either digital or analog (over-the-air aggregation) transmission and protected against interference using *frequency-hopping spread spectrum* (FHSS) following [25]. By analyzing the spatial convergence rate, we quantify the effects of network parameters on the learning performance for different transmission schemes and scenarios (i.e., low and high mobility). The key findings are summarized as follows.

- **Spatial convergence for digital transmission:** The spatial convergence rate (in terms of rounds) [26] is derived to quantify the deviation from the ground-true rate, which corresponds to direct gradient descent on the loss function. The deviation results from inter-cell interference and a random number of devices that succeed in transmission (i.e., a random data size), called *successful devices*. The key findings are as follows. First, as the device density grows, the expected number of successful devices converges to a

constant and thereby introduces a limit to the learning performance. The expected number is proportional to the processing gain of spread spectrum, decreases with a growing *signal-to-interference* (SIR) threshold for successful transmission, but is insensitive to variations of cell sizes. Second, the mentioned rate deviation diminishes *exponentially fast* as the expected number of successful devices increases. Last, channel-temporal diversity due to high mobility increases the chance of a device to succeed in transmission and participate in at least one round of the learning process, which increases the spatial-convergence rate.

- **Spatial convergence for analog transmission:** The distinctions of analog transmission is its support of simultaneous access while directly exposing the received model update to the perturbation by interference. The corresponding spatial convergence rate is derived by applying results on the interference distribution from stochastic geometry to the convergence analysis. The rate deviation from the ground truth reveals two conflicting effects of increasing the devices density. On one hand, without outage, the expected number of active devices participating in learning can grow unboundedly as the density increases. Consequently, more training data lead to faster spatial convergence. On the other hand, increasing the device density also causes the number of significant interferers to grow, which perturbs the SGD process and slows down spatial convergence. As the first scaling law is faster than the second, the net effect is found to be a higher spatial convergence rate when devices are denser. This makes analog transmission a favourable choice over the digital counterpart in a dense network.
- **Learning Latency:** Besides corroborating the above findings, experiments using a real dataset are conducted to compare the learning latency (in second) of digital and analog transmission. The latency of analog transmission is observed to be much lower than the digital-transmission counterpart in both sparse and dense networks. The low-latency of analog transmission in a sparse network results from more active devices (i.e., fewer rounds) and that in a dense network from shorter per-round latency. The findings are aligned with those for a single-cell system [9].

The remainder of this paper is organized as follows. Models and metrics are introduced in Section II. Spatial convergence is analyzed *with respect to* (w.r.t.) for the cases of digital-transmission and analog transmission in Sections III and IV, respectively. Experimental results are presented in Section V, followed by concluding remarks in Section VI.

II. MODELS AND METRICS

A. Network Topology Model

Adopting the classic model, the cellular network contains hexagonal cells as illustrated in Fig. 1 [27]. Base stations, denoted as $\{Y\} \subset \mathbb{R}^2$, are placed at cell centers. Let $C(Y, R)$ denote a cell centered at Y and with a distance R from Y to its boundary. Randomly located edge devices, denoted as $\{X\} \subset \mathbb{R}^2$, are randomly distributed on plane modeled as a homogeneous PPP $\Phi_d = \{X\}$ with density λ_d . FEEL is performed in a *typical cell* chosen by uniform sampling of all cells, denoted as $C_0 = C(Y_0, R)$ with Y_0 being the typical BS [17]. Devices in other cells are interferers involved in other services or tasks. To facilitate analysis, the number of devices in C_0 , namely $|\mathcal{C}_0 \cap \Phi_d|$, can be lower bounded by $K = |\mathcal{D}_0 \cap \Phi_d|$, where \mathcal{D}_0 represents the inscribed disk of C_0 with the radius R (see Fig. 1). For the K devices, their propagation distances to Y_0 are *independent and identically distributed* (i.i.d.) with the following *probability density function* (PDF):

$$f_R(r) = \frac{2r}{R^2}, \quad 0 < r < R. \quad (1)$$

Remark 1 (Extension to Random Cells). It is possible to extend the current results to the case of random cells generated by BSs distributed as a Poisson point process instead of a hexagonal lattice [20]. Similar to the current case, a random typical cell can be inner bounded by a disk but its radius, R , is now random. Specifically, R has the distribution function of $f_R(r) = 8\pi\lambda_s r \exp(-4\lambda_s \pi r^2)$ [20]. The current analytical results hold conditioned on a given R . Then taking their expectation with respect to the distribution of R yields the desired extension.

B. Federated Learning Model

The operations of FEEL is illustrated in Fig. 2 and described as follows. We consider the specific implementation of FEEL where stochastic gradients are computed at devices using local data and then transmitted to the server (co-located with the BS) for updating the global model [3] (see Remark 2 for extension to alternative implementation). Each round of FEEL comprises three phases: (1) global model updating and broadcasting, (2) local gradient computation, and (3) local gradient uploading. The current analysis focuses on the last phase as it represents the communication bottleneck of the FEEL system as discussed earlier. Let $t_{\text{cmm}}^{(n)}$ denote the duration of the uploading phase in the typical cell in the n -th round. The requirement that all participating

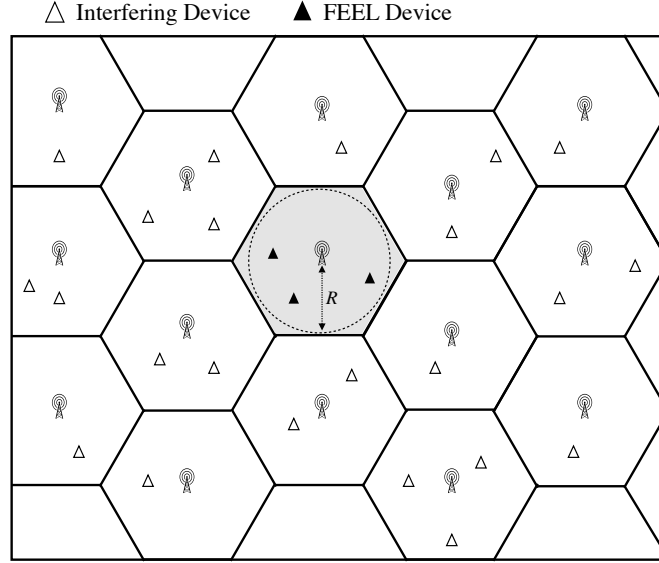


Fig. 1. The spatial model of a cellular network where FEEL is supported in a typical cell.

devices must finish their uploading within the duration before the global model can be updated introduces the constraint of so called synchronized updates [28]. Under the constraint, $t_{\text{cmm}}^{(n)}$ is a random variable depending on the random number of workers in the cell and their channel states. In contrast, the broadcasting phase uses the whole spectrum and can be assumed to finish within a given duration denoted as t_{bc} . Moreover, the workers are assumed to have comparable computation capacities, enabling them to complete local computation within a given duration denoted as t_{cmp} .

Let N denote the number of rounds needed for accomplishing the learning task, and $A^{(n)}$ the number of devices that successfully upload their gradients in the n -th round. Let I_X be an indicator function of worker X with $I_X = 1$ if transmission is successful or otherwise $I_X = 0$. Denote the device process in the n -th round as $\Phi_d^{(n)}$. Then we can write $A^{(n)} = \sum_{X \in \mathcal{C}_0 \cap \Phi_d^{(n)}} I_X$. Both the cases of high and low mobility are considered. In the case of high mobility, $\{\Phi_d^{(n)}\}$ are independent over different rounds and so are $\{A^{(n)}\}$. In the case of low mobility, they are fixed throughout the learning process: $\Phi_d^{(1)} = \Phi_d^{(2)} = \dots = \Phi_d^{(N)}$ and thus $A^{(1)} = A^{(2)} = \dots = A^{(N)}$.

In the current setting of supervised learning, let a labelled data sample be denoted as (\mathbf{u}, y) with \mathbf{u} and y representing the data and label, respectively. The samples follow an *unknown* probability distribution $p(\mathbf{u}, y)$. Let \mathbf{w} denote the model or its parameters. Consider the loss function $f(\mathbf{w}; \mathbf{u}, y)$, which measures the discrepancy between predicted output from \mathbf{w} using

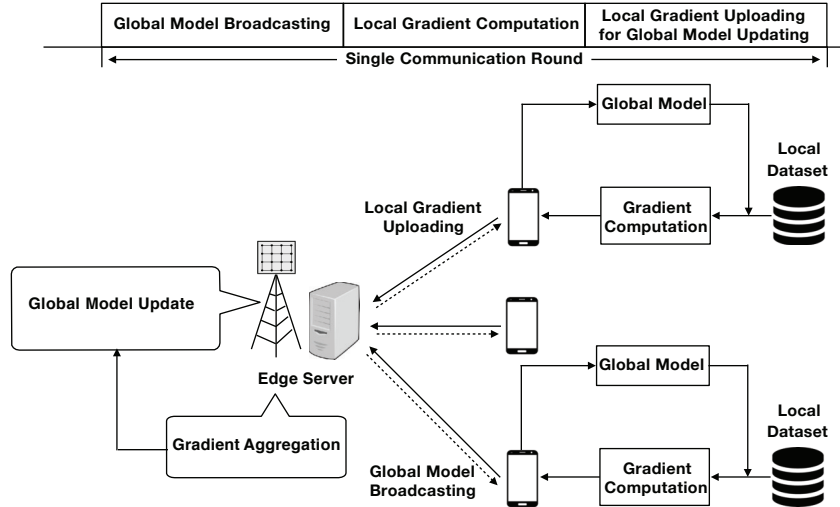


Fig. 2. The operations of FEEL in the typical cell.

the sample (\mathbf{u}, y) . The expected risk of the predictor \mathbf{w} , known as the *ground-true loss function*, is defined as [29]:

$$F(\mathbf{w}) = \mathbb{E}_{(\mathbf{u}, y) \sim p(\mathbf{u}, y)} [f(\mathbf{w}; \mathbf{u}, y)]. \quad (2)$$

Since the data distribution $p(\mathbf{u}, y)$ is unknown, it is impossible to find the ideal model $\mathbf{w}^* = \arg \min_{\mathbf{w}} F(\mathbf{w})$. FEEL is a distributed training algorithm for finding an approximate of the ideal model, which is described as follows.

To this end, some notation is introduced. The local dataset of device X is denoted as \mathcal{D}_X comprising samples that are drawn i.i.d. from $p(\mathbf{u}, y)$. Then the *local loss function* is defined in terms of the *empirical risk* as [11]:

$$F_X^{(n)}(\mathbf{w}^{(n)}) = \frac{1}{|\mathcal{D}_X|} \sum_{(\mathbf{u}, y) \in \mathcal{D}_X} f(\mathbf{w}^{(n)}; \mathbf{u}, y). \quad (3)$$

For convenience, we assume a uniform size for local datasets, i.e., $|\mathcal{D}_X| \equiv D, \forall X$. The learning task of the typical cell is specified by the tuple $\{F_0, F^*, f\}$, where f is the mentioned per-sample loss function, $F_0 \triangleq F(\mathbf{w}^{(0)})$ denotes the value of the ground-true loss function F at the initial model $\mathbf{w}^{(0)}$, and F^* is the global minimum of F .

The distributed SGD algorithm underpinning FEEL is described as follows (see e.g., [30]). Consider the n -th round, each device uses its local dataset \mathcal{D}_X and the model broadcast by the BS, $\mathbf{w}^{(n)}$, to compute the gradient of the local loss function $F_X^{(n)}(\mathbf{w}^{(n)})$, called a local gradient

and denoted as $\tilde{\mathbf{g}}_X^{(n)} = \nabla F_X^{(n)}(\mathbf{w}^{(n)})$. The local gradients are transmitted to the BS for averaging, yielding the following *global gradient estimate (of that of the ground-true loss function)*:

$$\bar{\mathbf{g}}_0^{(n)} = \begin{cases} \frac{1}{A^{(n)}} \sum_{X \in \mathcal{C}_0 \cap \Phi_d^{(n)}} \tilde{\mathbf{g}}_X^{(n)}, & A^{(n)} \geq 1, \\ 0, & A^{(n)} = 0. \end{cases} \quad (4)$$

It is applied to updating the global model based on gradient descent:

$$\mathbf{w}^{(n+1)} = \mathbf{w}^{(n)} - \mu \bar{\mathbf{g}}_0^{(n)}, \quad (5)$$

where the step size μ is called the *learning rate*. Last, the BS broadcasts the updated model to all devices, completing one round. The rounds are repeated till the model converges.

Remark 2 (Extension to Local-model Uploading). The current analysis can be extended to the alternative FEEL implementation with local-model uploading by accounting for multi-round local-gradient descent [3]. First, in each round, the local model at device X is updated via $\tilde{\mathbf{w}}_X^{(n+1)} = \mathbf{w}_X^{(n)} - \mu \tilde{\mathbf{g}}_X^{(n)}$; then $\tilde{\mathbf{w}}_X^{(n+1)}$ is transmitted to the server for updating the global model: $\mathbf{w}_X^{(n+1)} = \frac{1}{A^{(n)}} \sum_{X \in \mathcal{C}_0 \cap \Phi_d^{(n)}} \tilde{\mathbf{w}}_X^{(n+1)}$. The analysis can be modified accordingly and the modification is straightforward and does not change the findings.

For tractable convergence analysis, a set of assumptions commonly made in the literature (see e.g., [26]) are also adopted in this work.

Assumption 1. (Lower Bound) The ground-true loss function $F(\mathbf{w})$ is lower bounded, namely $F(\mathbf{w}) \geq F^*$ for some constant F^* .

Assumption 2. (Smoothness) Let S denote the model dimension and hence we can write the parameter vector as $\mathbf{w} = [w_1, w_2, \dots, w_S]^T$. The ground-true loss function $F(\mathbf{w})$ is assumed smooth. Mathematically, for the loss function evaluated at \mathbf{w} , we assume there exist a non-negative constant vector $\mathbf{L} := [L_1, L_2, \dots, L_S]^T$, the gradient of the ground-true loss function $F(\mathbf{w})$, $\nabla F(\mathbf{w})$, satisfies the following

$$|F(\boldsymbol{\beta}) - [F(\mathbf{w}) + \nabla F(\mathbf{w})^T(\boldsymbol{\beta} - \mathbf{w})]| \leq \frac{1}{2} \sum_{i=1}^S L_i (\beta_i - w_i)^2, \quad \forall \mathbf{w}, \boldsymbol{\beta}. \quad (6)$$

Define the \mathcal{L}_2 Lipschitz constant L_0 as $L_0 := \|\mathbf{L}\|_\infty = \max_i L_i$.

Assumption 3. (Variance Bound) The stochastic gradient (or local gradient estimate) $\tilde{\mathbf{g}}_X$ at an arbitrary device, say X , is an unbiased estimation of ground-true loss function and has a bounded variance:

$$\mathbb{E}[\tilde{\mathbf{g}}_X] = \nabla F \quad \text{and} \quad \mathbb{E}[\|\tilde{\mathbf{g}}_X - \nabla F\|^2] \leq \sigma^2, \quad (7)$$

where σ^2 is a given constant.

C. Uplink Transmission Models

The cellular network is assumed to be interference-limited, where channel noise is negligible. All BSs and devices are equipped with single antennas. The transmission power of a device in the typical cell depends on the specific transmission schemes as elaborated in the sequel. For simplicity, all interfering devices are assumed to fix their power as P . FHSS is adopted to regulate inter-cell interference [31]. Specifically, the total uplink bandwidth B is divided into M sub-carriers; each device randomly chooses one sub-carrier for transmission in each round and its choices over rounds are independent. As a result, the devices occupying an arbitrary sub-carrier, say sub-carrier m , is obtained from Φ_d by thinning and thus also a PPP but with density λ_d/M , denoted as $\hat{\Phi}_{d,m}$. The transmission by an arbitrary device, X , is received at the typical BS with the power $G_X|X - Y_0|^{-\alpha}$ where the coefficient $G_X = \exp(1)$ models Rayleigh fading and α denotes the path-loss exponent. All fading coefficients are assumed independent. We consider two transmission schemes for devices in the typical cell. They are described as follows.

1) *Digital Transmission:* For digital transmission, each coefficient of the local gradient at each device is quantized into a sufficiently large number of bits, denoted as D , such that the effect of quantization errors on learning performance is negligible. Then the quantized gradient is encoded and transmitted at the fixed rate $\frac{B}{M} \log(1 + \theta)$ with θ being a chosen constant. The fixed rate yields constant communication latency per round given as

$$t_{\text{cmm}} = \frac{SDM}{B \log(1 + \theta)}. \quad (8)$$

To cope with both intra-cell and inter-cell interference, all devices make independent choices of their hopping patterns, each of which refers to a sequence of choices of sub-carriers over rounds. Moreover, the transmission power of devices are assumed to be fixed and identical to

that of interferers. Considering the n -th round, the receive SIR for transmission by an arbitrary device in the typical cell, denoted as X_0 , over a chosen subcarrier, say m , can be written as:

$$\text{SIR}_{X_0}^{(n)} = \frac{G_{X_0}|X_0|^{-\alpha}}{\sum_{X \in \Phi_{d,m}^{(n)} \setminus \{X_0\}} G_X|X|^{-\alpha}}. \quad (9)$$

If the SIR exceeds the threshold θ , the uploaded gradient can be decoded correctly or otherwise an outage event occurs, resulting in the device being successful or inactive, respectively [32]. Let $\mathcal{A}^{(n)}$ denote the set of active (or successful) devices in the typical cell in the n -th round:

$$\mathcal{A}^{(n)} = \{X \in \Phi_d^{(n)} \cap \mathcal{C}_0 | \text{SIR}_X^{(n)} \geq \theta\}. \quad (10)$$

Then $A^{(n)} = |\mathcal{A}^{(n)}|$.

2) *Analog Transmission*: In each round, all devices in the typical cell transmit their local gradients using linear analog modulation without coding and over the same sub-carrier to perform over-the-air aggregation [28]. In other words, their hopping patterns are identical but independent of those of interferers. Following the model in [28], assuming i.i.d. data over devices, the distribution of the local-coefficients at each device is assumed to have the mean and variance, denoted as ν and $\tilde{\sigma}^2$, respectively, which are identical for all devices and known by them. To facilitate power control, a local-gradient vector at each device, say X , is normalized before transmission to have zero mean and unit variance, i.e., $\mathbf{s}_X^{(n)} = \frac{\tilde{\mathbf{g}}_X^{(n)} - \nu}{\tilde{\sigma}}$. Then the normalized vector is analog modulated and transmitted as $\sqrt{P_X} \mathbf{s}_X^{(n)}$, where P_X denotes the transmission power. Next, for the typical BS to receive a desired average of uploaded local gradients, their corresponding received signals must have aligned in magnitude, called *magnitude alignment* [28]. To this end, power control based on truncated channel inversion is applied to suppress channel fading [33]:

$$P_X = \begin{cases} \frac{\eta}{G_X|X|^{-\alpha}}, & G_X \geq g_{\text{th}}, \\ 0, & \text{otherwise,} \end{cases} \quad (11)$$

where η is the magnitude scaling factor of the received signal and g_{th} is a channel truncation threshold chosen to avoid exceeding an average power budget, denoted as $\bar{P} = \mathbb{E}[P_X]$. For fair performance comparison with digital transmission, we set the average transmission power to be $\bar{P} = P$ or equivalently $\mathbb{E}[P_X] = P$.

The two constants η and g_{th} are set such that the constraint of average transmission power can be satisfied [11], [33]. The reason for not factoring path loss into channel truncation is similar

to that for proportional fairness with the “fairness” measure modified as data diversity in the current context. In other words, preventing devices with high path loss from transmission would fail to exploit data distributed at the cell edge for learning, and thus scarifies data diversity; small-scale fading based truncation in (11) avoids such an issue. By reuse of notation, let $\mathcal{A}^{(n)}$ re-denotes the set of devices whose channels are not truncated in n -th round:

$$\mathcal{A}^{(n)} = \{X \in \Phi_d^{(n)} \cap \mathcal{C}_0 | G_X \geq g_{\text{th}}\}. \quad (12)$$

Then $A^{(n)} = |\mathcal{A}^{(n)}|$ is the number of active devices in the n -th round.

Given analog transmission, the received aggregated signal vector at the typical BS is

$$\mathbf{y}_0 = \sum_{X \in \mathcal{A}^{(n)}} \sqrt{P_X G_X} |X|^{-\frac{\alpha}{2}} \mathbf{s}_X^{(n)} + \mathbf{I}_0, \quad (13)$$

where \mathbf{I}_0 is the interference given as

$$\mathbf{I}_0 = \sum_{X' \in \hat{\Phi}_{d,m}^{(n)} \cap \bar{\mathcal{C}}_0} \sqrt{P_{X'} G_{X'}} |X'|^{-\frac{\alpha}{2}} \mathbf{s}_{X'}^{(n)}. \quad (14)$$

At the typical BS, the desired estimation of the aggregated gradient is obtained by the following de-normalization of the received signal [11], [33]:

$$\begin{aligned} \bar{\mathbf{g}}_0^{(n)} &= \frac{\tilde{\sigma}}{A^{(n)} \sqrt{\eta}} \mathbf{y}_0 + \nu \\ &= \frac{1}{A^{(n)}} \sum_{X \in \mathcal{A}^{(n)}} \tilde{\mathbf{g}}_X^{(n)} + \frac{\mathbf{I}_0 \tilde{\sigma}}{A^{(n)} \sqrt{\eta}}. \end{aligned} \quad (15)$$

Since the symbol duration is $T_s = \frac{M}{B}$, the per-round latency for the analog transmission is

$$t_{\text{cmm}} = \frac{SM}{B}. \quad (16)$$

D. Learning Performance Metrics

Two metrics for measuring the performance of FEEL in a spatial network are defined as follows. The first is the *spatial convergence criterion*. Consider FEEL in a specific cell centered at a fixed location $y \in \mathbb{R}^2$. Given N rounds, let $\mathcal{J}(N)$ denotes the index set of rounds with a non-empty cell and the number of *effective rounds* $N_e = |\mathcal{J}(N)|$. A convergence criterion widely adopted in the FEEL literature (see e.g., [26]) is determined by the expectation of averaged-gradient norm over rounds:

$$\bar{g}_0(N) = \mathbb{E} \left[\frac{1}{N_e} \sum_{n \in \mathcal{J}(N)} \|\nabla F(\mathbf{w}^{(n)})\|^2 \middle| N_e \geq 1 \right] \leq \varepsilon_0, \quad (17)$$

where ε_0 is a given constant. Note that the expectation in (17) is taken over the distribution of descent trajectories. Since the typical cell \mathcal{C}_0 results from uniform sampling of all cells, there exists a probability that the learning in the cell fails to meet the convergence criterion in (17): $\Pr(\bar{g}_0(N) > \varepsilon_0)$. The spatial convergence criterion is defined as one that the network can support model training within N rounds with a high probability, $(1 - \delta)$. Mathematically,

$$\Pr(\bar{g}_0(N) > \varepsilon_0) \leq \delta. \quad (18)$$

It is worth mentioning that if FEEL is performed in all cells, the probability in (18) can be interpreted as the percentage of cells where learning fails to be completed in time.

The next performance metric is *expected learning latency* defined as the expected time duration (in second) required for learning in the typical cell to meet the spatial convergence criterion in (18). Let N^* denote the smallest number of rounds for meeting the criterion. The expected learning latency is the expected sum of computation-and-communication latency over N rounds:

$$\bar{T}_\Sigma = \mathbb{E} \left[\sum_n^{N^*} t_{\text{cmm}}^{(n)} \right] + N^*(t_{\text{cmp}} + t_{\text{bc}}). \quad (19)$$

III. SPATIAL CONVERGENCE FOR THE DIGITAL-TRANSMISSION CASE

In this section, we consider the digital-transmission case and study the effects of network parameters on the spatial learning performance. To this end, we derive a sufficient condition for meeting the spatial convergence criterion and analyze the corresponding bound on the minimum expected learning latency. Both the cases of high and low mobility are considered.

A. Spatial Convergence Analysis with Low-Mobility

Consider FEEL in the typical cell with low mobility. For tractability, the analysis in this section focuses on the case where only the subset of devices lying in the inscribed circle of the cell [see Fig. 1 (a)], \mathcal{D}_0 , upload local gradients while other devices are silent. As it reduces training data, the corresponding convergence rate lower bounds the counterpart involving all devices.

First, we derive the distribution of the number of active (successful) devices in \mathcal{D}_0 . To this end, define the *success probability*, denoted as p_s , as the probability that an arbitrary device in \mathcal{D}_0 succeeds in transmission. Mathematically,

$$p_s = \mathbb{E}_X[\Pr(\text{SIR}_X^{(n)} > \theta | X \in \mathcal{D}_0)], \quad (20)$$

where $\text{SIR}_X^{(n)}$ is given in (9). Using the well-known Laplace-transform method (see e.g., [34]), the probability can be obtained as shown in the following lemma.

Lemma 1 (Success Probability [34]). The success probability of a typical device in the disc cell \mathcal{D}_0 is given as

$$p_s = \frac{1 - \exp(-aR^2)}{aR^2}, \quad (21)$$

where

$$a = \frac{2\pi\lambda_d \mathcal{B}\left(\frac{2}{\alpha}, 1 - \frac{2}{\alpha}\right) \theta^{\frac{2}{\alpha}}}{\alpha M}, \quad (22)$$

with $\mathcal{B}(x, y)$ being the beta function: $\mathcal{B}(x, y) = \int_0^1 t^{x-1}(1-t)^{y-1} dt$.

Let M_X denote an indicator whether device X is successful or not, i.e., $M_X = \mathbb{I}(\text{SIR}_X \geq \theta)$. Thereby, the success devices form a marked PPP represented by $\tilde{\Phi}_d = \{X, M_X\}$. By applying the theorem of marked PPP, the density of $\tilde{\Phi}_d$ is obtained as $\lambda_d p_s$ [18]. Let K denote the number of successful devices in \mathcal{D}_0 .

Lemma 2 (Distribution of the Number of Successful Devices). The distribution of the number of successful devices, K , is given as

$$\Pr(K = j) = \frac{\exp(-\bar{K}) (\bar{K})^j}{j!}, \quad (23)$$

with the mean

$$\bar{K} = \pi\lambda_d R^2 p_s = \frac{\alpha M (1 - e^{-aR^2})}{2\mathcal{B}\left(\frac{2}{\alpha}, 1 - \frac{2}{\alpha}\right) \theta^{\frac{2}{\alpha}}}, \quad (24)$$

and a is given in (22).

Remark 3 (Finite Active Devices). It should be emphasized that as the device density λ_d grows, the expected number of successful devices, \bar{K} , does not diverge since p_s decreases due to stronger interference according to Lemma 2. As a result, \bar{K} converges to a constant:

$$\bar{K} \rightarrow \frac{\alpha M}{2\mathcal{B}\left(\frac{2}{\alpha}, 1 - \frac{2}{\alpha}\right) \theta^{\frac{2}{\alpha}}}, \quad \lambda_d \rightarrow \infty. \quad (25)$$

In FEEL, increasing the number of successful devices has the effect of increasing the batch-size of training data. This reduces the variance of the global gradient estimate. Given Assumption 3, it is straightforward to quantify the reduction as shown in the following lemma.

Lemma 3. In the typical cell, the number of successful devices in the n -th round, $K^{(n)}$, reduces the variance of the global gradient estimate as follows:

$$\mathbb{E} \left[\left\| \frac{1}{K^{(n)}} \sum_{X \in K^{(n)}} \tilde{\mathbf{g}}_X^{(n)} - \nabla F(\mathbf{w}^{(n)}) \right\|^2 \right] \leq \frac{\sigma^2}{K^{(n)}}. \quad (26)$$

In low-mobility case, the number of successful devices in \mathcal{D}_0 is fixed throughout the learning process: $K^{(1)} = K^{(2)} = \dots = K^{(N)} = K$. Note that K is a random variable since the typical cell is a random process. With K fixed for a particular typical-cell realization, the model converge has been analyzed extensively in the literature. Specifically, the following result on the convergence rate can be derived using the method in [26].

Lemma 4 (Fixed-Cell Convergence with Digital Transmission and Low-mobility [26]). Consider the case with digital transmission and low mobility. With K fixed, and given the learning rate $\mu = \frac{1}{L_0\sqrt{N}}$, the expected averaged-gradient norm is bounded as follows:

$$\bar{g}_0(K, N) \leq \frac{1}{\sqrt{N}} \left[(F_0 - F^*) + \frac{\sigma^2}{K} \right], \quad K > 0. \quad (27)$$

Since K is a random variable, so is the averaged gradient norm. To facilitate spatial convergence analysis, we apply the Markov inequality to upper bound the norm as

$$\begin{aligned} \Pr(\bar{g}_0(K, N) > \varepsilon_0) &= \Pr(\bar{g}_0(K, N) > \varepsilon_0 \mid K > 0) (1 - p_{\text{null}}) + p_{\text{null}} \\ &\leq \frac{\mathbb{E}[\bar{g}_0(K, N) \mid K > 0]}{\varepsilon_0} (1 - p_{\text{null}}) + p_{\text{null}}, \end{aligned}$$

where the void probability $p_{\text{null}} = \Pr(K = 0)$. It follows from Lemma 2 that $p_{\text{null}} = e^{-\bar{K}}$. By setting the above upper bound equal to δ , a sufficient condition for meeting the spatial convergence criteria in (18) is

$$\mathbb{E}[\bar{g}_0(K, N) \mid K > 0] \leq \frac{(\delta - p_{\text{null}})\varepsilon_0}{1 - p_{\text{null}}}. \quad (28)$$

Consider a *typical non-empty* cell from uniformly sampling the set of non-empty cells. Then the spatial convergence rate of FEEL as measured using the metric $\mathbb{E}[\bar{g}_0(K, N) \mid K > 0]$ can be obtained as shown in the following theorem.

Theorem 1 (Spatial Convergence with Digital Transmission and Low-mobility). In this case, given the learning rate $\mu = \frac{1}{L_0\sqrt{N}}$, the expected averaged-gradient norm of a *typical non-empty* cell is bounded as follows:

$$\mathbb{E}[\bar{g}_0(K, N) \mid K > 0] \leq \frac{1}{\sqrt{N}} \left[(F_0 - F^*) + \frac{\sigma^2 e^{-\bar{K}}}{1 - e^{-\bar{K}}} (\text{Ei}(\bar{K}) - \log \bar{K} - \gamma) \right], \quad (29)$$

where \bar{K} is the expected number of active devices in (24), the exponential integral $\text{Ei}(x) = \int_{-\infty}^x \frac{\exp(t)}{t} dt$ and γ represents the Euler's Constant ($\approx 0.5772\dots$).

Proof. See Appendix A. □

At the right-hand side of (29), the first term, namely $(F_0 - F^*)$, represents gradient descent along a path defined by the ground-true gradients. On the other hand, the second term that is a function of \bar{K} reflects the effect of inaccurate distributed gradient estimation. Its dependance on \bar{K} is discussed as follows. According to Remark 3, in a network with dense devices, \bar{K} is independent of the device density but proportional to $M\theta^{-\frac{2}{\alpha}}$. Using the result, it follows from Theorem 1 that the deviation of convergence rate from the ideal one can be approximated as

$$\mathbb{E}[\bar{g}_0(K, N) \mid K > 0] - \frac{F_0 - F^*}{\sqrt{N}} \approx \frac{c_1 \sigma^2}{\sqrt{N}} \exp\left(-\frac{c_2 M}{\theta^{\frac{2}{\alpha}}}\right), \quad (30)$$

where c_1 and c_2 are constants. One can observe that the loss in convergence rate due to distributed gradient estimation decays at an exponential rate when either the number of sub-channels, M , or the SIR-threshold function $\theta^{-\frac{2}{\alpha}}$ increases. The gain of the former arises from interference suppression using FHSS and that of the latter from the reduction of outage probability as θ reduces, both of which contribute to the growth of the number of successful devices.

It should be emphasized that the above gains of convergence rate (in round) is at the cost of increased per-round latency (in second). The learning latency is discussed as follows.

Remark 4 (Learning Latency). For ease of notation, define the constant $\varepsilon = \frac{(\delta - p_{\text{null}})\varepsilon_0}{1 - p_{\text{null}}}$. Based on the result in Theorem 1, to meet the spatial-convergence criterion in (18), the expectation of the required number of round, denoted as N_{\min} , is upper bounded as

$$\mathbb{E}[N_{\min}] \leq \frac{1}{\varepsilon^2} \left[(F_0 - F^*) + \frac{\sigma^2 e^{-\bar{K}}}{1 - e^{-\bar{K}}} (\text{Ei}(\bar{K}) - \log \bar{K} - \gamma) \right]^2. \quad (31)$$

Then the expected learning latency defined in (19) is given as

$$\bar{T}_{\Sigma} = \mathbb{E}[N_{\min}] \cdot \underbrace{\left(\frac{SDM}{B \log(1 + \theta)} + t_{\text{cmp}} + t_{\text{bc}} \right)}_{\text{Per-round latency}}. \quad (32)$$

where t_{cmp} and t_{bc} are recalled to be constant latency for computation and broadcasting, respectively. The dependence of learning latency on network parameters are described as follows.

- (*SIR Threshold*) Increasing the SIR threshold θ is found to have two opposite effects. On one hand, a larger θ reduces the number of active devices and increases the null probability

p_{null} . This causes the increase of the required rounds for spatial convergence. On the other hand, increasing θ leads to a higher data rate and hence lower per-round latency. These effects give rise to the need optimizing θ for minimizing the learning latency as further illustrated by experimental results in the sequel.

- (*Device Density*) One can observe from (31) and (32) that the device density λ_d (or the expected number of active devices \bar{K}) affects only the expected number of rounds but not the per-round latency. As λ_d (or \bar{K}) increasing, the expected number of rounds converges to the minimum.
- (*Processing Gain*) Increasing the processing gain of FHSS, M , reduces the number of required rounds (via increasing the number of active devices) but *linearly* increases the per-round latency. When there is a sufficiently large number of active devices (i.e., sufficient exploited data), it is desirable to rein in the second effect by keeping M small.

B. Spatial Convergence Analysis with High Mobility

In this sub-section, we show that high mobility increases the spatial convergence rate as well as reduces the learning latency. In this case, the typical-cell realization changes independently over rounds. Consequently, an empty cell in one round can be non-empty in another. In contrast, the realization is fixed throughout the learning process in the case of low mobility. Therefore, for FEEL to be feasible, the typical cell in the current case should uniformly sample those cells that are *non-empty in at least one of N round*, i.e., $N_e > 0$. For the consistency with digital case and tractability, it is also necessary to choose a suitable learning rate as $\mu = \frac{1}{L_0} \sqrt{\mathbb{E} \left[\frac{1}{N_e} \mid N_e \geq 1 \right]}$. Then the spatial convergence rate is derived as follows.

Theorem 2 (Spatial Convergence with Digital Transmission and High-mobility). In this case, given the learning rate $\mu = \frac{1}{L_0} \sqrt{\mathbb{E} \left[\frac{1}{N_e} \mid N_e \geq 1 \right]}$ and small p_{null} , the expected averaged-gradient norm of the typical cell that is non-empty in at least one round is bounded as follows:

$$\mathbb{E}[\bar{g}_0(N) \mid N_e \geq 1] \leq \sqrt{\frac{1}{N} + \frac{p_{\text{null}}}{N-1}} \left[(F_0 - F^*) + \frac{\sigma^2 e^{-\bar{K}}}{1-e^{-\bar{K}}} (\text{Ei}(\bar{K}) - \log \bar{K} - \gamma) \right] + O(p_{\text{null}}^2), \quad (33)$$

where \bar{K} is defined in (24) and $\text{Ei}(\cdot)$ and γ follow those in Theorem 1.

Proof. See Appendix B. □

Comparing Theorems 1 and 2, when p_{null} is small, one can conclude that high mobility slightly reduces the spatial convergence rate, which is averaged over non-empty cells, approximately by

the factor of $\sqrt{1 + p_{\text{null}}}$. However, it should be emphasized that the percentage of non-empty cells in the case of high mobility is larger than that in the case of low mobility, namely $(1 - p_{\text{null}}^N)$ versus $(1 - p_{\text{null}})$. If all cells are considered, the opposite conclusion can be drawn based on the following learning-latency analysis.

To this end, the above result is applied to analyzing the learning latency in the case of high-mobility. Similar to (28), a sufficient condition for meeting the spatial convergence criterion in (18) is obtained as

$$\mathbb{E}[\bar{g}_0(N) \mid N_e \geq 1] \leq \frac{(\delta - p_{\text{null}}^N)\varepsilon_0}{1 - p_{\text{null}}^N}. \quad (34)$$

Using the condition, the learning latency is analyzed and compared with that in the case of low mobility as discussed in Remark 5.

Remark 5 (Learning Latency Comparison). For convenience, define the constant $\varepsilon' = \frac{(\delta - p_{\text{null}}^N)\varepsilon_0}{1 - p_{\text{null}}^N}$. Let N'_{\min} and \bar{T}'_{Σ} denote the required number of rounds and learning latency under the sufficient convergence conditions in (34). Then they can be derived using Theorem 2. Using the result and Remark 4, since per-round latency is identical for both the cases of low and high mobility, the ratio of corresponding expected latency is equal that of the expected numbers of required rounds:

$$\begin{aligned} \frac{\bar{T}'_{\Sigma}}{\bar{T}_{\Sigma}} &= \frac{\mathbb{E}[N'_{\min}]}{\mathbb{E}[N_{\min}]} \approx \frac{\varepsilon^2 \sqrt{1 + p_{\text{null}}}}{(\varepsilon')^2} \\ &\approx 1 - \left(\frac{2}{\delta} - \frac{5}{2}\right) p_{\text{null}}, \quad p_{\text{null}} \rightarrow 0. \end{aligned}$$

As suggested by the result, if δ is small, the learning latency (in second) with high mobility is slightly smaller than the low-mobility counterpart despite low-mobility having a faster convergence rate (in round) in non-empty cells. The reason is that in the former case, more cells are able to support FEEL and hence a more relaxed spatial convergence criterion. Note that the above analysis is based on approximation and bounds. Therefore, the actual quantification may not be accurate despite yielding the correct conclusion. More significant latency reduction due to high mobility is observed from experimental results in the sequel.

IV. SPATIAL CONVERGENCE FOR THE ANALOG-TRANSMISSION CASE

In the preceding section, spatial convergence of the FEEL is studied for the digital-transmission case. In this section, it is analyzed for the analog-transmission case that enables low-latency over-the-air aggregation. We assume low mobility. The extension of the results to the case of high

mobility is similar to that in the preceding section. As it yields no new insight, the details are omitted for brevity. By reuse of notation, identical symbols as used in the preceding section are also used to denote their counterparts in the current case whenever there is no confusion.

First, the distinction of the current case is the direct exposure of the received signal, namely over-the-air aggregated gradient, to inter-cell interference. The effect can be expressed mathematically by deriving the deviation of the aggregated gradient from the ground truth as follows. From (15), the expectation of aggregated gradient is an unbiased estimate of the ground truth:

$$\mathbb{E} \left[\bar{\mathbf{g}}_0^{(n)} \right] = \mathbb{E} \left[\frac{\mathbf{I}_0^{(n)} \tilde{\sigma}}{K \sqrt{\eta}} + \frac{1}{K} \sum_{X \in K} \tilde{\mathbf{g}}_X^{(n)} \right] = \nabla F(\mathbf{w}^{(n)}), \quad (35)$$

and its variance can be written as:

$$\begin{aligned} \mathbb{E} \left[\|\bar{\mathbf{g}}_0^{(n)} - \nabla F(\mathbf{w}^{(n)})\|^2 \right] &= \mathbb{E} \left[\left\| \frac{\mathbf{I}_0^{(n)} \tilde{\sigma}}{K \sqrt{\eta}} + \left(\frac{1}{K} \sum_{X \in K} \tilde{\mathbf{g}}_X^{(n)} - \nabla F(\mathbf{w}^{(n)}) \right) \right\|^2 \right] \\ &\leq \frac{\tilde{\sigma}^2 (\mathbf{I}_0^{(n)})^2}{\eta K^2} + \frac{\sigma^2}{K}, \end{aligned} \quad (36)$$

where K is the number of active devices in the inscribed cell, \mathcal{D}_0 , of the typical cell. Given (35) and (36), a similar result as in Lemma 4 can be obtained as follows.

Lemma 5 (Fixed-Cell Convergence with Analog Transmission and Low-mobility). In this case, consider a fixed cell with a given number of active devices, K , and the learning rate $\mu = \frac{1}{L_0 \sqrt{N}}$, the expected averaged-gradient norm is bounded as follows:

$$\bar{g}_0(K, N) \leq \frac{1}{\sqrt{N}} \left((F_0 - F^*) + \frac{\sigma^2}{K} + \frac{\tilde{\sigma}^2}{K^2 \eta N} \sum_{n=0}^{N-1} (\mathbf{I}_0^{(n)})^2 \right). \quad (37)$$

Accounting for the random distribution of K , the spatial-and-round averaged gradient norm follows from Lemma 5 as

$$\mathbb{E}[\bar{g}_0(K, N) \mid K > 0] \leq \frac{1}{\sqrt{N}} \left(F_0 - F^* + \sigma^2 \mathbb{E} \left[\frac{1}{K} \mid K > 0 \right] + \frac{\tilde{\sigma}^2}{\eta} \mathbb{E} \left[\frac{(\mathbf{I}_0^{(n)})^2}{K^2} \mid K > 0 \right] \right). \quad (38)$$

Next, to derive a closed-form expression for the above upper bound, it is necessary to analyze the distribution of K as follows. In the digital-transmission case, a device is activated based on the criterion of successful transmission. In the current case, given truncated channel inversion in (11), the criterion is for the device's fading gain to meet the truncation threshold. This results in the *activation probability* given as $p_a \triangleq \Pr(G_X \geq g_{\text{th}}) = e^{-g_{\text{th}}}$. It follows that

$$\Pr(K = j) = \frac{\exp(-\bar{K}') (\bar{K}')^j}{j!}, \quad (39)$$

where $\bar{K}' = \pi R^2 \lambda_d p_a$ is the expected number of active devices in the typical disk cell, \mathcal{D}_0 .

Using (38) and (39), we derive the main result of this section as follows.

Theorem 3 (Spatial Convergence with Analog Transmission and Low-mobility). In this case, given the learning rate $\mu = \frac{1}{L_0 \sqrt{N}}$, the expected averaged-gradient norm of a typical *non-empty* cell is bounded as follows:

$$\mathbb{E}[\bar{g}_0(K, N) \mid K > 0] \leq \frac{1}{\sqrt{N}} \left[(F_0 - F^*) + \sigma^2 \phi + \frac{16\tilde{\sigma}^2(-\text{Ei}(-g_{\text{th}}))}{p_a(\alpha^2 - 4)M} \left(\phi - \frac{\bar{K}' e^{-\bar{K}'}}{1 - e^{-\bar{K}'}} \right) \right], \quad (40)$$

with

$$\phi = \mathbb{E} \left[\frac{1}{K} \mid K > 0 \right] = \frac{e^{-\bar{K}'}}{1 - e^{-\bar{K}'}} [\text{Ei}(\bar{K}') - \log(\bar{K}') - \gamma], \quad (41)$$

where the expected number of active devices $\bar{K}' = \pi R^2 \lambda_d p_a$, the exponential integral Ei and Euler's Constant γ follow those in Theorem 1, and the term $(-\text{Ei}(-g_{\text{th}}))$ is positive.

Proof. See Appendix C. □

The second term on the right-hand side of (40), $\sigma^2 \phi$, represents the error of distributed gradient estimation and is observed to have the same form as its counterpart for the digital-transmission case in Theorem 1 but with \bar{K} replaced by \bar{K}' . Due to the different scalings of \bar{K} and \bar{K}' w.r.t. the device density λ_d , there is an important difference between the two cases. Specifically, as the density λ_d increases, the term for the case of analog transmission diminishes at an *exponential rate* while its digital-transmission counterpart converges to a *constant* according to (25). This results in different accuracies of distributed gradient estimation. On the other hand, analog transmission exposes learning to the effect of inter-cell interference as represented by the last term in (40). Though higher density will cause larger interference, one can observe that this term also decays at an exponential rate as λ_d grows. The fundamental reason is that more devices are involved with the increasing density and the interference can be effectively suppressed by gradient aggregation. Combining the above discussion suggests that analog transmission is preferred to digital transmission in a network with dense devices as also corroborated by experimental results.

Next, we compare the relative effects of interference and distributed-data induced gradient deviations from the ground truth. To this end, we consider the following ratio between the last two terms of (40), called *interference effect*:

$$\frac{\text{Interference induced deviation}}{\text{Data induced deviation}} = \frac{16\tilde{\sigma}^2(-\text{Ei}(-g_{\text{th}}))}{\sigma^2 p_a (\alpha^2 - 4) M} \cdot \left(1 - \frac{\bar{K}'}{\text{Ei}(\bar{K}') - \log(\bar{K}') - \gamma} \right). \quad (42)$$

The dependence of interference effect on different network parameters is discussed as follows.

- (*Device-density/cell-size*) Increasing the device density or cell size both lead to linear growth of the expected number of devices, \bar{K}' . This reduces the interference effect in two aspects. One is the suppression of interference by more aggressively averaging via over-the-air aggregation. The other is larger path-loss for interference signals received at the BS. Mathematically, the interference reduction by increasing the cell size is reflected in the last term on the right hand side of (42), $\left(1 - \frac{\bar{K}'}{\text{Ei}(\bar{K}') - \log(\bar{K}') - \gamma}\right)$, being a decreasing function of \bar{K}' .
- (*Path-loss exponent*) The interference effect is observed to diminish as the path-loss exponent α increases, which reduces inter-cell interference by reducing spatial coupling between cells.
- (*Processing gain*) The interference effect is inversely proportional to the processing gain of FHSS, M . Though the increase of M seems to accelerate learning (in terms of rounds), it increases per-round latency (in second) as the effective transmission bandwidth, namely B/M , reduces. See more discussion in the sequel.
- (*Channel truncation threshold*) The interference effect decreases as a decreasing threshold causes the activation probability to grow. This holds only in the considered interference-limited regime. Reducing the threshold may not be desired in the noise-limited regime as it can cause devices with weak channels to participate in learning, amplifying the noise effect.

Similar to the analysis shown in the digital case, given the spatial convergence target δ and the null probability p_{null} , a sufficient condition for meeting the spatial convergence criterion in (18) is obtained as

$$\text{E}[\bar{g}_0(K, N) \mid K > 0] \leq \frac{(\delta - p_{\text{null}})\varepsilon_0}{1 - p_{\text{null}}}. \quad (43)$$

Remark 6 (Learning Latency). Under the sufficient condition in (43), the expected minimum number of rounds, denoted as $\text{E}[N_{\text{min}}]$, has no simple form but can be upper bounded by the ratio between the upper bound on the averaged-gradient norm in Theorem 3 and the constant $\varepsilon = \frac{(\delta - p_{\text{null}})\varepsilon_0}{1 - p_{\text{null}}}$. The expected learning latency can be written as

$$\bar{T}_{\Sigma} = \text{E}[N_{\text{min}}] \cdot \underbrace{\left(\frac{SM}{B} + t_{\text{cmp}} + t_{\text{bc}}\right)}_{\text{Per-round latency}}, \quad (44)$$

where t_{cmp} and t_{bc} are recalled to be constant computation and broadcasting latency, respectively. One key observation is that increasing the processing gain M increases per-round latency but

reduces the expected number of rounds as mentioned earlier. This suggests the need of optimizing M for latency minimization.

V. EXPERIMENTAL RESULTS

A. Experimental Settings

The experimental settings are as follows unless specified otherwise. Consider a cellular network in a 50×50 (unit area) horizontal area. Each hexagon cell's radius is 1 (unit length). FEEL is deployed in the cell located at the centre of the area. The path-loss exponent is set as $\alpha = 4$, and total bandwidth is $B = 1$ MHz. In the digital-transmission case, we assume that each coefficient of a transmitted gradient is quantized into 16 bits; in the analog-transmission case, each coefficient is mapped to a symbol. Transmission power in digital case is given by $P = 1$ for all the edge devices, while in the analog case, η and g_{th} are set to satisfy the average power constraint $E[P_X] = P$. The constant computing-and-broadcasting latency is assumed negligible in our experiments. Let each sample path be a sequence of typical-cell realizations over rounds. Then each result on spatially averaged learning performance (i.e., test accuracy or learning latency) is computed as the average of 10 sample paths to account for spatial network distribution.

The learning task is to perform the handwritten-digit recognition using the well-known MNIST dataset. There are total 60,000 labeled training data samples in this dataset, each edge device is assigned 200 samples by randomly sampling the dataset. The classifier model is implemented using a 6-layer *convolutional neural network* (CNN) that consists of two 5×5 convolution layers with ReLU activation, each followed by 2×2 max pooling, a fully-connected layer with 512 units, ReLU activation, and a final softmax output layer.

B. Effect of Device Mobility

Consider the case of digital transmission. The curves of spatially averaged test accuracy versus the number of rounds are plotted in Fig. 3 for both the cases of low and high mobility. Overall, one can observe that convergence rate with high mobility is faster than the low-mobility counterpart, which is aligned with the theoretic analysis. In particular, when devices are sparse (i.e., $\lambda_d = 1$), the test accuracy with low mobility (0.9) is substantially lower than that with high mobility (> 0.95). The reason is that the data size and diversity are both insufficient, which, however, can be effectively overcome by mobility. The benefit of mobility in terms of convergence rate

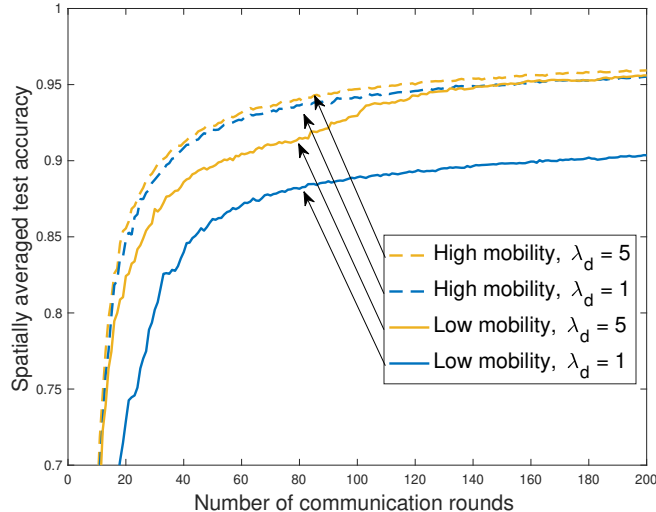


Fig. 3. The spatially averaged test accuracy versus the number of communication rounds for both the cases of digital transmission with low and high mobility and a varying device density λ_d .

can also be observed even for a higher density, i.e., $\lambda_d = 5$. The difference attributed to mobility diminishes when the density is sufficiently high ($\lambda_d = 10$).

C. Effects of Network Parameters

Consider the case of digital transmission. The effects of network parameters, namely the device density, SIR threshold, and processing gain, on learning latency are demonstrated in Fig. 4. The curves of spatially averaged learning latency versus network parameters are plotted for achieving the target spatially averaged test accuracy of 95%. Several observations can be made. First, one can observe from Fig. 4(a) that the learning latency decreases and then saturates as λ_d increases. The first part corresponds to the data-limited regime where increasing the density of devices contributes more training data and thereby reducing the needed number of rounds. The second part corresponds to the data-sufficient regime where more devices no longer yield an increase of the convergence rate. Second, it can be observed from Fig. 4(b) that the latency first decreases and then increases as the SIR threshold θ grows. This corroborates Remark 4 based on analysis and suggests the need of optimizing θ . Last, Fig. 4(c) shows the linear growth of latency as the processing gain M increases. Thus, for the current experimental settings, the minimum processing gain ($M = 1$) is desired. This is aligned with Remark 4.

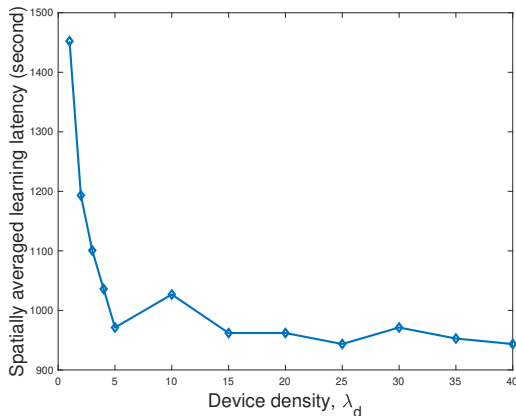
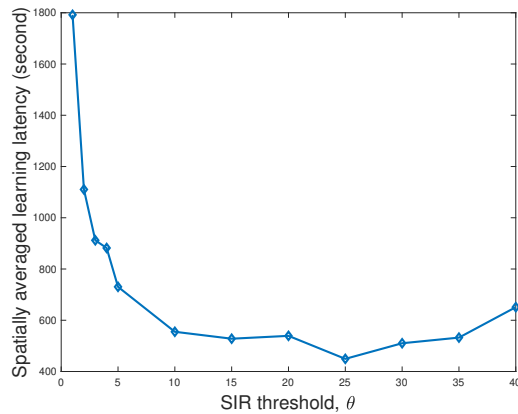
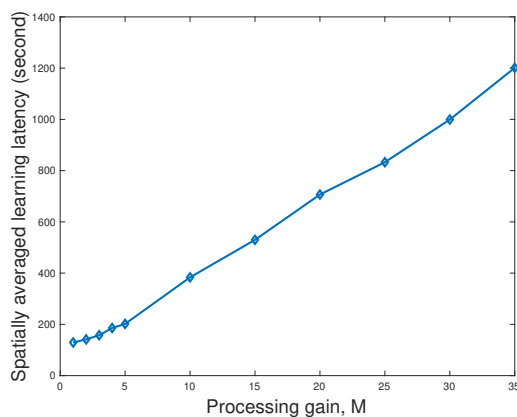
(a) Effect of device density λ_d (b) Effect of SIR threshold θ (c) Effect of processing gain M

Fig. 4. The effects of network parameters on learning latency with digital transmission for achieving a target spatially averaged test accuracy of 95%.

D. Comparison of Digital and Analog Transmission

The spatially averaged test accuracies for the cases of digital and analog transmission are compared in Fig. 5 in terms of spatially averaged test accuracy. Different device densities are considered. When the network is relatively sparse (i.e., $\lambda_d = 1$ or 3), digital transmission is observed to outperform the analog scheme as the latter exposes uncoded signals to the perturbation of inter-cell interference. On the other hand, when there are many active devices (i.e., $\lambda_d = 30$), the aggressive over-the-air aggregation realized by analog transmission effectively suppresses interference by averaging. Consequently, analog transmission achieves better performance in this case.

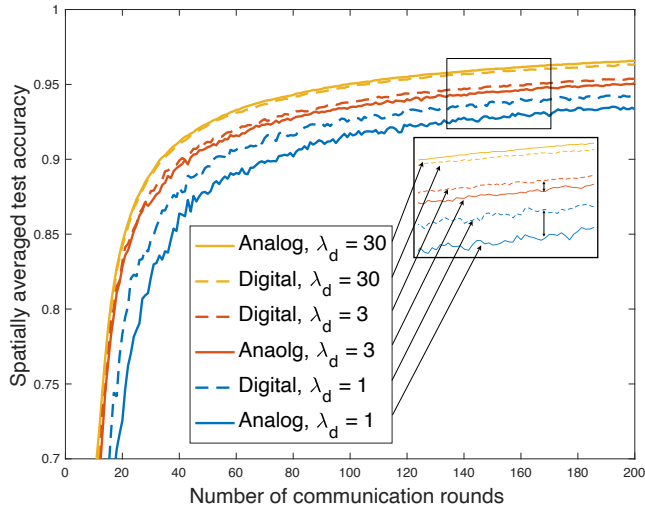


Fig. 5. Comparison of spatially averaged test accuracies for the cases of digital and analog transmission for different device densities.

The learning performance for the cases of digital and analog transmission is further compared in Fig. 6 in terms of the required number of rounds and spatially averaged learning latency for the target spatially averaged test accuracy of 93%. The learning latency for analog transmission is observed from Fig. 6(a) to be much lower than the digital-transmission counterpart for both low- and-high device densities. One can observe from Fig. 6(b) that in a sparse network ($\lambda_d \leq 10$), error-free transmission of digital transmission reduces the required number of rounds; in a dense network ($\lambda_d \geq 10$), the gain vanishes as analog transmission supports more active devices. Regardless of this difference in terms of required rounds, the advantage of shorter per-round latency of analog transmission dominates, resulting in the earlier observation from Fig. 6(a).

VI. CONCLUDING REMARKS

In this work, we have investigated the spatial convergence of FEEL deployed in a typical cell of a large-scale cellular network. Both the schemes of digital and analog transmission are considered. In terms of spatial convergence rate (in round), digital transmission is preferred for low-to-medium device densities while convergence with analog transmission is faster when devices are dense. On the other hand, in terms of learning latency (in second), analog transmission is always preferred due to its support of low-latency over-the-air aggregation.

This work opens the direction of distributed edge learning in large-scale cellular networks, in which numerous topics warrant further investigation. In particular, a more complex network

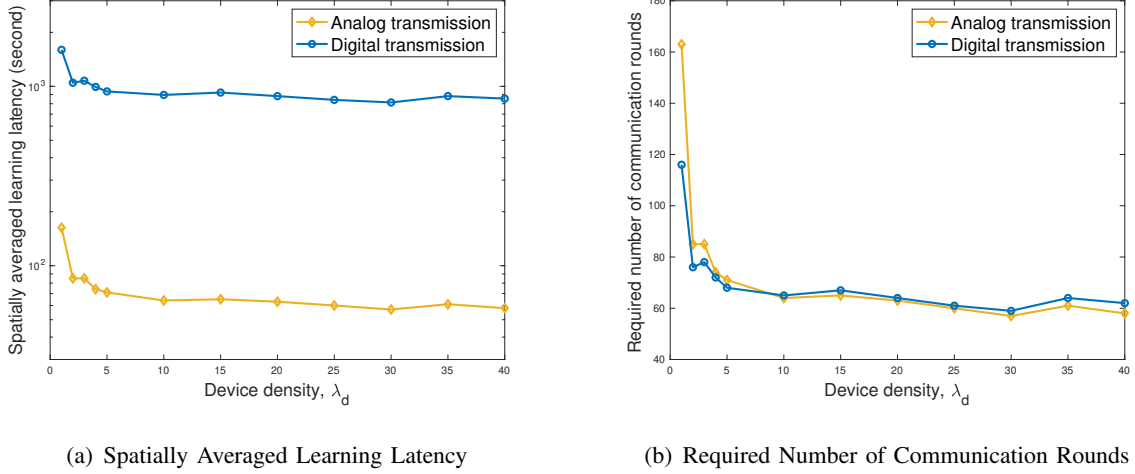


Fig. 6. Learning-performance comparison between the cases of digital and analog transmission in terms of: (a) spatially averaged learning latency and (b) the required number of rounds for the targeted spatially averaged test accuracy of 95%.

topology including both backhaul and radio-access links can be considered to support hierarchical federated learning involving edge devices, edge servers and central-cloud servers. Moreover, the current work suggests the need of optimizing network parameters (e.g., SIR threshold), which can be further investigated to improve the learning performance. Furthermore, for the deployment of FEEL in 5G networks, it is interesting to study the effects of advanced physical-layer techniques (i.e., massive MIMO and non-orthogonal access) on the spatial learning performance.

APPENDIX A

PROOF OF THEOREM 1

It follows from Lemma 4 that

$$\mathbb{E}[\bar{g}_0(K, N) \mid K > 0] \leq \frac{1}{\sqrt{N}} \left((F_0 - F^*) + \sigma^2 \mathbb{E} \left[\frac{1}{K} \mid K > 0 \right] \right). \quad (45)$$

Using the distribution of K in Lemma 2, the last term in (45) can be obtained as follows

$$\begin{aligned} \mathbb{E} \left[\frac{1}{K} \mid K > 0 \right] &= \sum_{j=1}^{\infty} \frac{1}{j} p(A = j \mid A > 0) \\ &= \frac{\exp(-\pi R^2 \lambda_d p_s)}{1 - \exp(-\pi R^2 \lambda_d p_s)} \sum_{j=1}^{\infty} \frac{1}{j} \frac{(\pi R^2 \lambda_d p_s)^j}{j!} \\ &\stackrel{(b)}{=} \frac{\exp(-\pi R^2 \lambda_d p_s)}{1 - \exp(-\pi R^2 \lambda_d p_s)} \left(\text{Ei}(\pi R^2 \lambda_d p_s) - \log(\pi R^2 \lambda_d p_s) - \gamma \right), \quad (46) \end{aligned}$$

where (b) is obtained using [35, (3.16)]. The desired result follows.

APPENDIX B
PROOF OF THEOREM 2

First, we analyze the convergence in the typical cell condition on its being non-empty. Based on Assumption 2 and substituting (5) into (6), the single-step improvement of the loss function is obtained as

$$\begin{aligned} F(\mathbf{w}^{(n+1)}) - F(\mathbf{w}^{(n)}) &\leq (\nabla F(\mathbf{w}^{(n)}))^T (\mathbf{w}^{(n+1)} - \mathbf{w}^{(n)}) + \sum_{i=1}^d \frac{L_i}{2} (\mathbf{w}^{(n+1)} - \mathbf{w}^{(n)})_i^2 \\ &\leq -\mu (\nabla F(\mathbf{w}^{(n)}))^T \bar{\mathbf{g}}^{(n)} + \frac{\|L\|_\infty}{2} \mu^2 \|\bar{\mathbf{g}}^{(n)}\|^2, \end{aligned} \quad (47)$$

where $\bar{\mathbf{g}}^{(n)}$ is the aggregated gradient received at the BS in the n^{th} round. Note that two random processes underpinning the spatial learning process are $\{K^{(n)}; n \geq 0\}$ and $\{\bar{\mathbf{g}}^{(n)}; n \geq 0\}$. Consider the $(n+1)^{\text{th}}$ communication round, condition on fixed $K^{(n)} > 0$ and the model updated in the preceding round, taking expectation of both sides of (47) yields

$$\begin{aligned} \mathbb{E} [F(\mathbf{w}^{(n+1)}) - F(\mathbf{w}^{(n)}) | K^{(n)}] &\leq -\mu (\nabla F(\mathbf{w}^{(n)}))^T \left(\frac{1}{K^{(n)}} \sum_{X \in \mathcal{D}_0^{(n)}} \mathbb{E} [\tilde{\mathbf{g}}_X^{(n)}] \right) \\ &\quad + \frac{L_0 \mu^2}{2} \mathbb{E} \left[\left\| \frac{1}{K^{(n)}} \sum_{X \in \mathcal{D}_0^{(n)}} \tilde{\mathbf{g}}_X^{(n)} \right\|^2 \middle| K^{(n)} \right], \end{aligned} \quad (48)$$

where $L_0 = \|L\|_\infty$. Based on Assumption 3 and Lemma 3, (48) can be written as:

$$\begin{aligned} \mathbb{E} [F(\mathbf{w}^{(n+1)}) - F(\mathbf{w}^{(n)}) | K^{(n)}] &\leq -\mu \|\nabla F(\mathbf{w}^{(n)})\|^2 + \frac{L_0 \mu^2}{2} \left(\|\nabla F(\mathbf{w}^{(n)})\|^2 + \frac{\sigma^2}{K^{(n)}} \right) \\ &= \left(-\mu + \frac{L_0 \mu^2}{2} \right) \|\nabla F(\mathbf{w}^{(n)})\|^2 + \frac{L_0 \mu^2 \sigma^2}{2K^{(n)}}. \end{aligned} \quad (49)$$

Conditioning on the effective number of rounds $N_e \geq 1$, performing a telescoping sum over the iterations gives

$$\begin{aligned} F_0 - F^* &\geq F_0 - \mathbb{E}[F(\mathbf{w}^{(n)}) | N_e \geq 1] \\ &= \mathbb{E} \left[\sum_{n=0}^{N_e-1} (F(\mathbf{w}^{(n)}) - F(\mathbf{w}^{(n+1)})) \middle| N_e \geq 1 \right] \\ &\geq \left(\mu - \frac{L_0 \mu^2}{2} \right) \sum_{n=0}^{N_e-1} \|\nabla F(\mathbf{w}^{(n)})\|^2 - \frac{L_0 \mu^2 \sigma^2}{2} \sum_{n=0}^{N_e-1} \frac{1}{K^{(n)}}, \quad N_e \geq 1. \end{aligned} \quad (50)$$

Since N_e is a random variable, it follows that

$$(F_0 - F^*)\mathbb{E} \left[\frac{1}{N_e} \middle| N_e \geq 1 \right] \geq \left(\mu - \frac{L_0\mu^2}{2} \right) \mathbb{E} \left[\frac{1}{N_e} \sum_{n=0}^{N_e-1} \|\nabla F(\mathbf{w}^{(n)})\|^2 \middle| N_e \geq 1 \right] - \frac{L_0\mu^2\sigma^2}{2} \mathbb{E} \left[\frac{1}{N_e} \sum_{n=0}^{N_e-1} \frac{1}{K^{(n)}} \middle| N_e \geq 1 \right].$$

By rearranging the terms,

$$\mathbb{E} \left[\frac{1}{N_e} \sum_{n=0}^{N_e-1} \|\nabla F(\mathbf{w}^{(n)})\|^2 \middle| N_e \geq 1 \right] \leq \frac{(F_0 - F^*)\mathbb{E} \left[\frac{1}{N_e} \middle| N_e \geq 1 \right] + \frac{L_0\mu^2\sigma^2}{2} \mathbb{E} \left[\frac{1}{N_e} \sum_{n=0}^{N_e-1} \frac{1}{K^{(n)}} \middle| N_e \geq 1 \right]}{\mu - L_0\mu^2/2}. \quad (51)$$

On the other hand, since $\mu = \frac{1}{L_0} \left(\mathbb{E} \left[\frac{1}{N_e} \middle| N_e \geq 1 \right] \right)^{1/2}$,

$$\begin{aligned} \frac{1}{\mu - L_0\mu^2/2} &= \frac{2L_0}{\left(\mathbb{E} \left[\frac{1}{N_e} \middle| N_e \geq 1 \right] \right)^{1/2} \left(2 - \left(\mathbb{E} \left[\frac{1}{N_e} \middle| N_e \geq 1 \right] \right)^{1/2} \right)} \\ &\stackrel{(a)}{\leq} \frac{2L_0}{\left(\mathbb{E} \left[\frac{1}{N_e} \middle| N_e \geq 1 \right] \right)^{1/2}}, \end{aligned} \quad (52)$$

where (a) follows from $\left(\mathbb{E} \left[\frac{1}{N_e} \middle| N_e \geq 1 \right] \right)^{1/2} \leq 1$. By combining (51) and (52), and replacing $\mathbb{E} \left[\frac{1}{N_e} \sum_{n=0}^{N_e-1} \|\nabla F(\mathbf{w}^{(n)})\|^2 \middle| N_e \geq 1 \right]$ with $\bar{g}_0(N)$,

$$\bar{g}_0(N) \leq \left(\mathbb{E} \left[\frac{1}{N_e} \middle| N_e \geq 1 \right] \right)^{1/2} \left((F_0 - F^*) + \sigma^2 \mathbb{E} \left[\frac{1}{N_e} \sum_{n=0}^{N_e-1} \frac{1}{K^{(n)}} \middle| N_e \geq 1 \right] \right). \quad (53)$$

For spatial convergence, take expectation over the spatial distribution of edge devices, one can obtain the following upper bound on the spatial-and-round averaged gradient:

$$\mathbb{E}[\bar{g}_0(N) \mid N_e \geq 1] \leq \left(\mathbb{E} \left[\frac{1}{N_e} \middle| N_e \geq 1 \right] \right)^{1/2} \left((F_0 - F^*) + \sigma^2 \mathbb{E} \left[\frac{1}{K^{(n)}} \middle| K^{(n)} > 0 \right] \right). \quad (54)$$

The expression for the term in (54), $\mathbb{E} \left[\frac{1}{N_e} \middle| N_e \geq 1 \right]$, can be obtained as

$$\begin{aligned} \mathbb{E} \left[\frac{1}{N_e} \middle| N_e \geq 1 \right] &= \sum_{i=1}^N \frac{1}{i} \binom{N}{i} \frac{(1 - p_{\text{null}})^i (p_{\text{null}})^{N-i}}{1 - p_{\text{null}}^N} \\ &\stackrel{(a)}{=} \frac{1}{1 - p_{\text{null}}^N} \sum_{i=1}^N \frac{p_{\text{null}}^{i-1} - p_{\text{null}}^N}{N - i + 1} \\ &= \frac{1}{N} + \frac{p_{\text{null}}}{N-1} + O(p_{\text{null}}^2), \quad p_{\text{null}} \rightarrow 0, \end{aligned} \quad (55)$$

where (a) is based on (10) in [36]. Substituting (55) and (46) into (54) yields the desired result.

APPENDIX C

PROOF OF THEOREM 3

Starting from (38), the proof focuses on deriving an expression for the perturbation term caused by inter-cell interference, namely $\frac{\tilde{\sigma}^2}{\eta} \mathbb{E} \left[\frac{(\mathbf{I}_0^{(n)})^2}{K^2} \middle| K > 0 \right]$. Due to the independence between the interference $(\mathbf{I}_0^{(n)})^2$ and the number of devices K ,

$$\frac{\tilde{\sigma}^2}{\eta} \mathbb{E} \left[\frac{(\mathbf{I}_0^{(n)})^2}{K^2} \middle| K > 0 \right] = \frac{\tilde{\sigma}^2}{\eta} \mathbb{E} \left[(\mathbf{I}_0^{(n)})^2 \right] \mathbb{E} \left[\frac{1}{K^2} \middle| K > 0 \right]. \quad (56)$$

First, by applying Campbell's Theorem [18],

$$\mathbb{E} \left[(\mathbf{I}_0^{(n)})^2 \right] = \frac{2\pi\lambda_d P R^{2-\alpha}}{(\alpha - 2)M}. \quad (57)$$

Next,

$$\begin{aligned} \mathbb{E} \left[\frac{1}{K^2} \middle| K > 0 \right] &= \mathbb{E} \left[\left(1 + \frac{1}{K}\right)^2 \cdot \frac{1}{(K+1)^2} \middle| K > 0 \right] \\ &\leq 4 \mathbb{E} \left[\frac{1}{(K+1)^2} \middle| K > 0 \right]. \end{aligned} \quad (58)$$

Using the distribution of K in (39),

$$\begin{aligned} \mathbb{E} \left[\frac{1}{K^2} \middle| K > 0 \right] &\leq \frac{4}{1 - \exp(-\bar{K}')} \sum_{j=1}^{\infty} \frac{\exp(-\bar{K}') (\bar{K}')^j}{(j+1)^2 j!} \\ &= \frac{4}{1 - \exp(-\bar{K}')} \left(\sum_{j=0}^{\infty} \frac{\exp(-\bar{K}') (\bar{K}')^j}{(j+1)^2 j!} - \exp(-\bar{K}') \right) \\ &= \frac{4}{1 - \exp(-\bar{K}')} \left(\frac{1}{\bar{K}'} \sum_{j=1}^{\infty} \frac{\exp(-\bar{K}') (\bar{K}')^j}{j j!} - \exp(-\bar{K}') \right) \\ &= \frac{4}{\bar{K}'} \mathbb{E} \left[\frac{1}{K} \middle| K > 0 \right] - \frac{\exp(-\bar{K}')}{1 - \exp(-\bar{K}')}. \end{aligned} \quad (59)$$

Combining (56), (57), and (59) gives

$$\frac{\tilde{\sigma}^2}{\eta} \mathbb{E} \left[\frac{(\mathbf{I}_0^{(n)})^2}{K^2} \middle| K > 0 \right] \leq \frac{8P\tilde{\sigma}^2}{\eta p_s (\alpha - 2) M R^\alpha} \cdot \left(\mathbb{E} \left[\frac{1}{K} \middle| K > 0 \right] - \frac{\bar{K}' e^{-\bar{K}'}}{1 - e^{-\bar{K}'}} \right). \quad (60)$$

On the other hand, based on truncated channel inversion in (11), the expected transmission power of a device is obtained as

$$\begin{aligned} \mathbb{E}[P_X] &= \mathbb{E} \left[\frac{\eta}{G_X |X|^{-\alpha}} \right] \\ &= \eta \mathbb{E} \left[\frac{1}{G_X} \right] \cdot \int_0^R r^\alpha f_R(r) dr \\ &= \frac{2\eta R^\alpha (-\text{Ei}(-g_{\text{th}}))}{\alpha + 2}. \end{aligned} \quad (61)$$

Under the average power constraint $E[P_X] = P$,

$$\eta = \frac{P(\alpha + 2)}{2R^\alpha(-\text{Ei}(-g_{\text{th}}))}. \quad (62)$$

Substituting (62) into (60) gives the desired result.

REFERENCES

- [1] Z. Zhou, X. Chen, E. Li, L. Zeng, K. Luo, and J. Zhang, "Edge intelligence: Paving the last mile of artificial intelligence with edge computing," *Proc. of the IEEE*, vol. 107, no. 8, pp. 1738–1762, 2019.
- [2] G. Zhu, D. Liu, Y. Du, C. You, J. Zhang, and K. Huang, "Toward an intelligent edge: wireless communication meets machine learning," *IEEE Comm. Magazine*, vol. 58, no. 1, pp. 19–25, 2020.
- [3] W. Y. B. Lim, N. C. Luong, D. T. Hoang, Y. Jiao, Y.-C. Liang, Q. Yang, D. Niyato, and C. Miao, "Federated learning in mobile edge networks: A comprehensive survey," *IEEE Commun. Surveys Tuts.*, 2020.
- [4] M. Chen, Z. Yang, W. Saad, C. Yin, H. V. Poor, and S. Cui, "A joint learning and communications framework for federated learning over wireless networks," *IEEE Trans. Wireless Commun.*, vol. 20, no. 1, pp. 269–283, 2021.
- [5] W. Shi, S. Zhou, Z. Niu, M. Jiang, and L. Geng, "Joint device scheduling and resource allocation for latency constrained wireless federated learning," *IEEE Trans. Wireless Commun.*, vol. 20, no. 1, pp. 453–467, 2021.
- [6] J. Ren, Y. He, D. Wen, G. Yu, K. Huang, and D. Guo, "Scheduling in cellular federated edge learning with importance and channel awareness," 2020. [Online]. Available: arXiv:2004.00490v2
- [7] Z. Yang, M. Chen, W. Saad, C. S. Hong, M. Shikh-Bahaei, H. V. Poor, and S. Cui, "Delay minimization for federated learning over wireless communication networks," 2020. [Online]. Available: <https://arxiv.org/abs/2007.03462>
- [8] J. Song and M. Kountouris, "Optimal number of edge devices in distributed learning over wireless channels," in *IEEE Workshop on Signal Process. Adv. Wireless Commun. (SPAWC) (virtual)*, May 26-29, 2020.
- [9] G. Zhu, J. Xu, and K. Huang, "Over-the-air computing for wireless data aggregation in massive IoT," 2020. [Online]. Available: <https://arxiv.org/abs/2009.02181>
- [10] M. M. Amiri and D. Gündüz, "Machine learning at the wireless edge: Distributed stochastic gradient descent over-the-air," *IEEE Trans. Signal Process.*, vol. 68, pp. 2155–2169, 2020.
- [11] G. Zhu, Y. Du, D. Gündüz, and K. Huang, "One-bit over-the-air aggregation for communication-efficient federated edge learning: Design and convergence analysis," *to appear in IEEE Trans. Wireless Commun.*, 2020.
- [12] N. Zhang and M. Tao, "Gradient statistics aware power control for over-the-air federated learning in fading channels," 2020. [Online]. Available: <https://arxiv.org/abs/2003.02089>
- [13] K. Yang, T. Jiang, Y. Shi, and Z. Ding, "Federated learning via over-the-air computation," *IEEE Trans. Wireless Commun.*, vol. 19, no. 3, pp. 2022–2035, 2020.
- [14] Y. Lin, S. Han, H. Mao, Y. Wang, and W. J. Dally, "Deep gradient compression: Reducing the communication bandwidth for distributed training," 2017. [Online]. Available: <https://arxiv.org/abs/1712.01887>
- [15] M. M. Amiri and D. Gündüz, "Federated learning over wireless fading channels," *IEEE Trans. Wireless Commun.*, vol. 19, no. 5, pp. 3546–3557, 2020.
- [16] H. H. Yang, Z. Liu, T. Q. Quek, and H. V. Poor, "Scheduling policies for federated learning in wireless networks," *IEEE Trans. Commun.*, vol. 68, no. 1, pp. 317–333, 2019.
- [17] M. Haenggi, J. G. Andrews, F. Baccelli, O. Dousse, and M. Franceschetti, "Stochastic geometry and random graphs for the analysis and design of wireless networks," *IEEE J. Sel. Areas Commun.*, vol. 27, no. 7, pp. 1029–1046, 2009.

- [18] J. Kingman, *Poisson Processes*, ser. Oxford Studies in Probability. United Kingdom: Oxford University Press, 1993.
- [19] S. N. Chiu, D. Stoyan, W. S. Kendall, and J. Mecke, *Stochastic geometry and its applications*. John Wiley & Sons, 2013.
- [20] J. G. Andrews, F. Baccelli, and R. K. Ganti, "A tractable approach to coverage and rate in cellular networks," *IEEE Trans. Commun.*, vol. 59, no. 11, pp. 3122–3134, 2011.
- [21] K. Hosseini, W. Yu, and R. S. Adve, "A stochastic analysis of network MIMO systems," *IEEE Trans. Signal Process.*, vol. 64, no. 16, pp. 4113–4126, 2016.
- [22] H. S. Dhillon, R. K. Ganti, F. Baccelli, and J. G. Andrews, "Modeling and analysis of K-tier downlink heterogeneous cellular networks," *IEEE J. Sel. Areas Commun.*, vol. 30, no. 3, pp. 550–560, 2012.
- [23] Y. S. Soh, T. Q. Quek, M. Kountouris, and H. Shin, "Energy efficient heterogeneous cellular networks," *IEEE J. Sel. Areas Commun.*, vol. 31, no. 5, pp. 840–850, 2013.
- [24] V. V. Chetlur and H. S. Dhillon, "Downlink coverage analysis for a finite 3-D wireless network of unmanned aerial vehicles," *IEEE Trans. Commun.*, vol. 65, no. 10, pp. 4543–4558, 2017.
- [25] S. P. Weber, Xiangying Yang, J. G. Andrews, and G. de Veciana, "Transmission capacity of wireless ad hoc networks with outage constraints," *IEEE Trans. Inf. Theory*, vol. 51, no. 12, pp. 4091–4102, 2005.
- [26] J. Bernstein, Y.-X. Wang, K. Aizzadenesheli, and A. Anandkumar, "signsgd: Compressed optimisation for non-convex problems," in *Int. Conf. Mach. Learn. (ICML)*, pp. 560–569, Stockholm, Sweden, 2018.
- [27] T. S. Rappaport, *Wireless Communications: Principles and Practice*, 1st ed. IEEE Press, 1996.
- [28] G. Zhu, Y. Wang, and K. Huang, "Broadband analog aggregation for low-latency federated edge learning," *IEEE Trans. Wireless Commun.*, vol. 19, no. 1, pp. 491–506, 2019.
- [29] J. Konečný, "Stochastic, distributed and federated optimization for machine learning," 2017. [Online]. Available: <https://arxiv.org/pdf/1707.01155.pdf>
- [30] B. McMahan, E. Moore, D. Ramage, S. Hampson, and B. A. y Arcas, "Communication-efficient learning of deep networks from decentralized data," in *Proc. Int. Conf. Artif. Int. Statist. (AISTATS)*, pp. 1273–1282, Ft. Lauderdale, FL, Apr. 20 - 22, 2017.
- [31] A. Goldsmith, *Wireless Communications*. USA: Cambridge University Press, 2005.
- [32] S. Weber, J. G. Andrews, and N. Jindal, "The effect of fading, channel inversion, and threshold scheduling on ad hoc networks," *IEEE Trans. Inf. Theory*, vol. 53, no. 11, pp. 4127–4149, 2007.
- [33] X. Cao, G. Zhu, J. Xu, and K. Huang, "Optimized power control for over-the-air computation in fading channels," *IEEE Trans. Commun.*, vol. 19, no. 11, pp. 7498–7513, 2020.
- [34] J. G. Andrews, A. K. Gupta, and H. S. Dhillon, "A primer on cellular network analysis using stochastic geometry," 2016. [Online]. Available: <https://arxiv.org/pdf/1604.03183.pdf>
- [35] M.-T. Chao and W. Strawderman, "Negative moments of positive random variables," *J. Amer. Stat. Assoc.*, vol. 67, no. 338, pp. 429–431, 1972.
- [36] F. F. Stephan, "The expected value and variance of the reciprocal and other negative powers of a positive bernoullian variate," *Ann. Math. Stat.*, vol. 16, no. 1, pp. 50–61, 1945.